2019 IEEE/RSJ International Conference on Intelligent Robots and Systems (IROS)
Macau, China, November 4-8, 2019

Design and Verification of A Portable Master Manipulator Based on an Effective Workspace Analysis Framework

Dandan Zhang, *Student Member, IEEE*, Jindong Liu, *Senior Member, IEEE*, Lin Zhang
Guang-Zhong Yang, *Fellow, IEEE*

***Abstract*— Master manipulators represent a key component of Robot-Assisted Minimally Invasive Surgery (RAMIS). In this paper, an Analytic Hierarchy Process (AHP) method is used to construct an effective workspace analysis framework, which can assist the configuration selection and design evaluation of a portable master manipulator for surgical robot control and training. The proposed framework is designed based on three criteria: 1) compactness, 2) workspace quality, and 3) mapping efficiency. A hardware prototype, called the Hamlyn Compact Robotic Master (Hamlyn CRM), is constructed following the proposed framework. Experimental verification of the platform is conducted on the da Vinci Research Kit (dVRK) with which a da Vinci robot is controlled as a slave. The proposed Hamlyn CRM is compared with Phantom Omni, a commercial portable master device, with results demonstrating the relative merits of the new platform in terms of task completion time, average control speed and number of clutching.**

I. Introduction

The therapeutic success of emerging robotic platforms for Minimally Invasive Surgery (MIS) has spurred the field of robotic surgery under constant evolution [1]. This tendency echoes both research and commercial efforts to further develop technologies for robotic surgery [2], with the aim of bringing more tangible benefits to the healthcare system [3].

A typical robotic surgery system consists of three major components: a master control console for interactive manipulation, a slave surgical robot with actuation instruments, and a feedback system with vision and other sensing modalities. Master-slave control is used extensively for human-robot interaction for robotic surgery. The master-slave paradigm allows motion scaling and tremor removal while retaining direct control of the user through a slave robot to complete a surgical task. The performance of the master-slave robotic system depends on the capability of its master device to seamlessly relay a surgeon's manoeuvre to the slave robot.

The da Vinci surgical system is now the global market leader for robotic surgery [4]. Except for the da Vinci Surgical System, most of the current surgical robots occupy a large footprint in the operating room, which is not practical to realize widespread clinical uptake. This has inspired the development of smarter and smaller systems in recent years [5]. With the current drive of developing surgical robots towards smarter and smaller systems [5], e.g., LER robot [6], CURES robot [7], and Micro-IGES robot [8], it is desirable to develop compact and portable master manipulators. For practical deployment in hospitals, these compact systems can be easily fitted within the general surgical environments.

In general, master manipulators can be classified as joint-space master manipulators and task-space master manipulators [9]. A joint-space master manipulator has a similar kinematic structure as the slave robot's arm, so the arm motion of the operator can be directly mapped to the slave robot using joint-to-joint mapping. Although they have certain advantages in terms of intuitive control, they lack generalizability for wider applications, which is the strength of task space manipulators. Another classification is to divide master robots into serial robots and parallel robots. As for parallel robots, they have the advantage of high precision control, but their smaller workspace is often a major limitation for practical use. To track the 3D position and 3D orientation of the human hand, the master manipulator should have at least six Degrees of Freedom (DoFs). The 3D orientation of the hand is realized by the flexibility of the wrist and it can be mimicked by three DoFs, with their axes intersected at a common point. The other three DoFs can be used to sense the position of the end-effector. This design is known as position and orientation decoupling. In this paper, the coupled design configuration will not be considered. Therefore, a task space serial master manipulator with a decoupling design for teleoperation is the main focus of this paper.

Among task-space master serial manipulators, some existing products have already incorporated a compact design. These include, for example, the Phantom Omni (Geomagic Touch), which is widely adopted as a general-purpose master controller in many research systems. Actaeon (BBZ) [10], a lightweight and portable control console, is developed for surgical training. A passive master manipulator with a Remote Centre of Motion (RCM) mechanism is designed for minimally invasive surgery [11]. However, there is a lack of a systematic approach for evaluating the design of master manipulators. An optimized configuration of the master manipulator is essential to improve the performance of teleoperation. A surgical robot system will be difficult to realize its full potential if paired with an unsuitable remote controller [9]. Therefore, an overall analysis framework for master manipulators is required.

As for configuration selection, there are sixteen different kinematic configurations available for potential master manipulators to realize position control [12]. Generally, they can be summarized into Cartesian robots, SCARA robots, cylindrical robots, spherical robots, and articulated robots.

All authors are with the Hamlyn Centre for Robotic Surgery, Imperial College London, London, United Kingdom. G.-Z. Yang is also with the Institute of Medical Robotics, Shanghai Jiao Tong University, China. Corresponding author email: d.zhang17@imperial.ac.uk

978-1-7281-4004-9/19/$31.00 ©2019 IEEE

Most of the slave robots for keyhole surgery have a spherical workspace. The reachable workspace of the spherical manipulators with RRP (two revolute joints, one prismatic joint) and the articulated robots with RRR (three revolute joints) configuration form a part of a sphere. Therefore, spherical robots and articulated robots are considered as the basic configurations for comparison in this paper.

The structure of the rest of the paper is organized as follows. Firstly, the effective workspace analysis framework is illustrated in Section II. Secondly, a systematic overview of the Hamlyn CRM is provided by detailing the structure design and control system in Section III. Thirdly, user studies are conducted to assess the relative performance of the Phantom Omni and the Hamlyn CRM with results analysis in Section IV. Finally, conclusions are drawn in Section V.

II. Methodology

In this section, the configuration selection for the master manipulator is introduced. Compactness, workspace quality and mapping efficiency are three main criteria for evaluation. A case study is provided to compare two candidates for determination of the configuration for the Hamlyn CRM.

A. Equivalent Model for Case Study

To make sure that the two robots are comparable during the configuration selection process, an equivalent model is proposed to enable the comparison to be independent of scale. Fig. 1 shows the kinematic structure of an articulated robot and a spherical robot, including the Denavit−Hartenberg (DH) table with joint limits. They are used as a pair of robots for the case study in this paper. We denote henceforth the link length of the first and second arm of the articulated robot as L_1 and L_2 respectively, the lower and upper joint limits for the spherical robot is L_3 and L_4 respectively. In addition, α,β,R are used to determine the end-effector position for the spherical robot in the spherical coordinate, where α and β represent the azimuth and inclination, R represents the radius and the link offset of the prismatic joint of the spherical robot. The corresponding joint values for the first three revolute joints of the articulated robot to reach the same position as the spherical robot can be calculated as α, $\beta \pm arccos\frac{(L_1^2+R^2-L_2^2)}{2L_1R}$ and $\pm(\pi - arccos\frac{(L_1^2+L_2^2-R^2)}{2L_1L_2})$. This equivalent relationship is demonstrated in Fig. 1.

Both of the articulated robot and the spherical robot have spherical reachable workspace provided that there are no physical limitations of the joint actuators. However, in reality, the reachable workspace of a robot is significantly reduced because of joint limits and not being able to form the shape of a sphere.

As a result, the shape and volume of the reachable workspace for the two types of robots will not be the same. The actual reachable workspace with joint limits is formed by the outside envelope surface and the inside envelope surface generated by the end-effector of the manipulator (see Fig. 2).

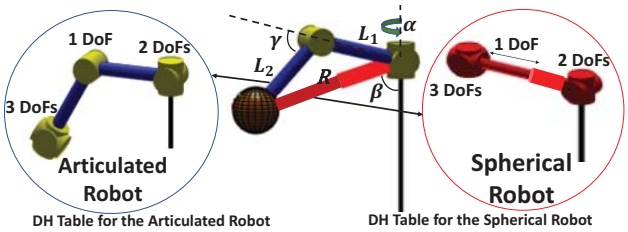

DH Table for the Articulated Robot

	1	2	3	4	5	6
α	0	90	-90	0	-90	90
a	0	0	0.2	0.2	0	0
d	0	0	0	0	0	0
θ	θ_1	θ_2	θ_3	θ_4	θ_5	θ_6
θ_u	45	135	0	180	160	70
θ_d	-45	45	-120	-180	20	-70

DH Table for the Spherical Robot

	1	2	3	4	5	6
α	0	90	-90	0	-90	90
a	0	0	0	0	0	0
d	0	0	d	0	0	0
θ	θ_1	θ_2	0	θ_4	θ_5	θ_6
θ_u	45	135	0.4	180	160	70
θ_d	-45	45	0.2	-180	20	-70

Fig. 1: An equivalent model for an articulated robot and a spherical robot. Note: The unit for the angle of the revolute joint is degree, while the unit for the link length, the link offset and the joint limits for prismatic joint are metre. θ_u and θ_d represents the upper and lower joint limits respectively.

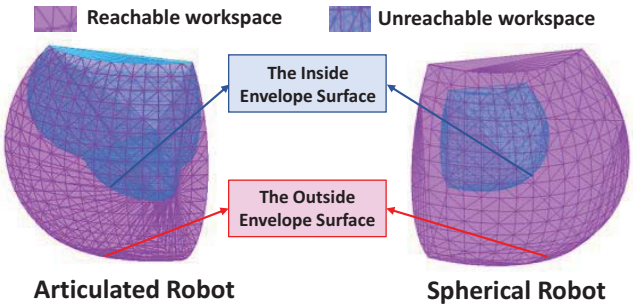

Fig. 2: Reachable workspace comparison between the articulated robot and the spherical robot.

Suppose that D_1 and D_2 represent the minimal distance between the base of the robot to the inside and outside envelope surface of the reachable workspace respectively. If both robots share the same value of D_1 and D_2, the influence of the dimension can be overlooked during the evaluation. They can be regarded as comparable master manipulators that satisfy the equivalent model during the configuration selection process, which is determined by (1).

$$\begin{cases} L_1 + L_2 = L_4 \\ \gamma = \pi - arccos(\frac{L_1^2+L_2^2-L_3^2}{2L_1L_2}) \end{cases} \tag{1}$$

B. Compactness

In practice, it is important for the operator to conduct remote control with minimal repositioning times using a master manipulator. That is to say, sufficient workspace volume is also important. For a compact master manipulator design, there should be a compromise between the volume of the workspace and the total link length and offset. A master manipulator with minimal link length and joint offset, but covering the targeted workspace can be regarded as a

valuable compact design. Compactness of the master manipulator can be improved by both kinematic structure and joint mechanism selection.

Suppose that a_i and d_i represent the link length and link offset of the i_{th} joint respectively, n_q is the number of joints for the robot, and V is the workspace volume. Structural length index ($S_l = \frac{1}{\sqrt[3]{V}}\sum_{i=1}^{n_q}(a_i + d_i)$) is based on the ratio of the manipulator length sum to the cube root of the workspace volume [12]. However, the link length for both robots and the link offset for the articulated robot are fixed, while the link offset d_i for the spherical robot is varying at different point during position control. Therefore, we proposed a modified index to evaluate the overall compactness.

Qualitatively, the arm of the spherical robot has less total link offset than the articulated one when $R < (L_1 + L_2)$, because of the principle of triangular relationship (see Fig. 1). To quantitatively evaluate the compactness of both of the robots, we assume that the actual link offset can be written as $d_i(x, y, z)$ for joint i_{th} when the end-effector of a robot is located at point $P(x, y, z)$ in the Cartesian Space. For an articulated robot, $d_i(x, y, z)(i = 1, 2...6)$ is fixed value given by the DH table. As for spherical robot, $d_i(x, y, z)(i = 3)$ is a variable determined by the prismatic joint, while the remaining joint offsets are fixed value. L_c is defined to evaluate the average actual length sum of a manipulator in (2).

$$L_c = \frac{1}{V}\iiint \sum_{i=1}^{n_q}(a_i + d_i(x, y, z))\, dx\, dy\, dz \tag{2}$$

The overall compactness C is based on the ratio of the cube root of the workspace volume to the average actual length, summed over the whole workspace. This is defined as follows.

$$C = \frac{\sqrt[3]{V}}{L_c} \tag{3}$$

The bigger the C value is, the higher the overall compactness can be obtained, and the higher portability of the robot can be ensured while sufficient workspace is guaranteed at the same time.

C. Workspace Quality

Manipulability, Inversed Condition Number and Minimum Singular Value are three common evaluation indices to analyze the workspace quality across the whole reachable workspace. The definitions are shown as follows.

- **Manipulability** ($M(\boldsymbol{q})$) : Manipulability represents the distance of a given pose of the manipulator to a singular configuration. It can evaluate the ability of the end-effector for the master manipulator to move in arbitrary directions [13].
- **Inversed Condition Number** ($C(\boldsymbol{q})$) : Condition number represents the distance to the kinematic isotropy of the Jacobian [14]. Inversed condition number is used to measure the degree of ill-conditioning of the manipulator.
- **Minimum Singular Value** ($S(\boldsymbol{q})$) : Minimum singular value represents an upper bound for the velocity with which the manipulator can move in all directions [14]. It is a good indicator of the closeness to singularities.

$$\begin{cases} M(\boldsymbol{q}) = \sqrt{det(J(\boldsymbol{q})J(\boldsymbol{q})^T)} \\ C(\boldsymbol{q}) = \frac{1}{||J(\boldsymbol{q})||\cdot||J(\boldsymbol{q})^{-1}||} \\ S(\boldsymbol{q}) = \sigma_{min}(\boldsymbol{q}) \end{cases} \tag{4}$$

where $\boldsymbol{q}$ is the joint value vector, $J(\boldsymbol{q})$ is the Jacobian matrix of the manipulator. By using the singular value decomposition, the Jacobian matrix can be decomposed to $\sigma_i(i = 1, 2...m)$. Therefore, $\sigma_{min} = min(\sigma_1, \sigma_2, \ldots, \sigma_m)$.

As joint limits may influence the evaluation metrics mentioned above, a penalization term $P(\boldsymbol{q})$ can be added to consider the impact of joint limits [15], [16].

$$P(\boldsymbol{q}) = 1 - exp(-K\prod_{i=1}^{n_q}\frac{(\theta_i - \theta_{id})(\theta_{iu} - \theta_i)}{(\theta_{iu} - \theta_{id})^2}) \tag{5}$$

where K is a scaling factor, θ_i is the joint angle, θ_{iu} and θ_{id} are the upper and lower bounds of the joint limit for the i_{th} joint respectively.

For overall evaluation, global modified indices are used for assessment. The global modified index G with joint limits can be defined as the integral of the normalized local index over the whole reachable workspace (see (6)).

$$G = \iiint T(\frac{F(\boldsymbol{q})P(\boldsymbol{q})}{F_{max}})\, dx\, dy\, dz \tag{6}$$

where $F(\boldsymbol{q})$ can be replaced by local indices $M(\boldsymbol{q})$, $C(\boldsymbol{q})$ or $S(\boldsymbol{q})$ to obtain the global modified index of manipulability, inversed condition number and minimum singular value respectively. F_{max} is the maximum value over the whole workspace for a specific index, and $T(.)$ is a mapping function from the joint space to the Cartesian space which can be realized through forward kinematics. The larger the G value is, the better quality of the workspace of the robot has, and thus the higher overall workspace quality can be achieved.

D. Mapping Efficiency

Master-slave mapping represents the kinematic correlation between the master controller and the slave robot, which is significant to be considered for teleoperation. Clutching is often required to reposition the end-effector of the master manipulator, due to the usual dissimilarities of the two workspaces. However, the frequent use of the clutching mechanism may influence the continuity of the clinical workflow. Therefore, mapping efficiency is utilized to evaluate the design of the master manipulator in this paper. Mapping efficiency can be evaluated by the geometric similarity of the workspace between the master robot and the slave robot.

For keyhole surgery, the trocar limits the motion of manipulators because of the fulcrum effect. Only one translational movement insertion displacement along the longitudinal axis, one rotational movement of the tool, and two rotational movements at the fulcrum point can be provided [17]. Rigid surgical tools inserted through the trocar within the abdominal cavity, are therefore contained by a cone with a vertex angle of sixty degrees during operation [18], [19].

To quantify the geometric similarity between the workspace of the master and the slave robot, the workspace of the master manipulator is scaled down by a fixed scaling ratio τ. The reasonable value of τ is determined by the targeted surgery. In this paper, we assume $\tau = 0.25$ for calculation. To conduct geometric similarity analysis, the workspace of the master and slave robot are overlapped together in the same coordinate system when the first revolute joint is aligned.

Suppose that α is the rotation angle of a virtual plane that goes through the rotational axis of the first revolute joint and intersected with the scaled down workspace of a robot, a corresponding characteristic graph $C(\alpha)$ for the section can be obtained. The effective area is defined as an area generated by the virtual plane when it intersects the reachable workspace. Fig. 3 (a) and (c) show the effective area of the articulated robot and the spherical robot respectively. Obviously, the effective area of the slave robot is a sector, as shown in Fig. 3 (b).

Intersection area can be calculated after overlapping the characteristic graph of the scaled down workspace of the master robot and that of the slave robot, as shown in Fig. 3 (d) and (e). The intersection area of the characteristic graph is utilized as a feature, while the intersection volume can be obtained through the integral of the intersection area over the workspace, which can be known as the common reachable workspace of the master and the slave robot.

TABLE I: Mapping Efficiency.

τ	0.1	0.15	0.2	0.25	0.3	0.35	0.4
Articulated	0.10	0.23	0.38	0.57	0.71	0.77	0.90
Spherical	0.12	0.25	0.40	0.56	0.74	0.88	0.83

In this paper, $P_I(\alpha, \theta, \rho)$ and $P_s(\alpha, \theta, \rho)$ represent the point within the interaction volume and the point within the effective volume of the slave robot respectively, where θ and ρ indicate the polar angle and radius in the polar coordinate of the characteristic graph $C(\alpha)$, respectively. A measure of workspace similarity S can be calculated as follows:

$$S = \frac{\iiint P_I(\alpha, \theta, \rho)\, d\alpha\, d\theta\, d\rho}{\iiint P_S(\alpha, \theta, \rho)\, d\alpha\, d\theta\, d\rho} \tag{7}$$

S reflects the ratio of the intersection volume of the master and slave robot to the slave robots effective volume within the unit sphere. The mapping efficiency may vary based on the choice of different scaling ratio, while the average value is used as the final mapping efficiency for evaluation. Table I shows the corresponding mapping efficiency under different given scaling ratio τ. The bigger the average similarity value is, the higher the similarity between the workspace of the master manipulator and the slave robot have, the more intuitive control can be realized.

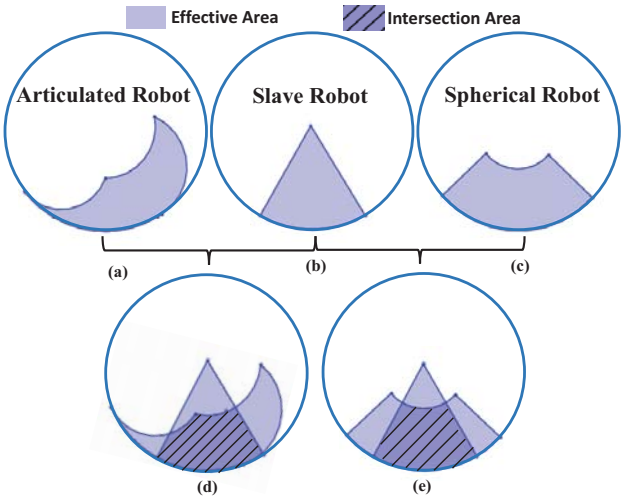

Fig. 3: Characteristic graphs for similarity analysis. Characteristic graph with effective area visualization of (a) the articulated master robot, (b) the slave robot, (c) the spherical master robot; overlapping area visualization between the slave robot and (d) the articulated master robot, (e) the spherical master robot.

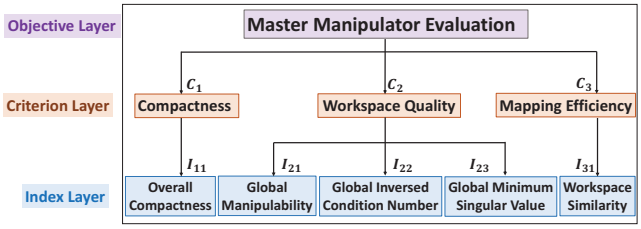

Fig. 4: Diagram for the construction of the AHP based effective workspace analysis framework.

E. Effective Workspace Analysis

For effective workspace analysis, it is necessary to take all the aforementioned factors into consideration. Due to the many factors involved, it is necessary to formulate a systematic framework for determining these parameters. To this end, AHP is used to determine the weights of different metrics [20]. Diagram for the construction of the AHP based effective workspace analysis framework is shown as Fig. 4. AHP is based on pairwise comparisons by comparing elements i and j, obtaining the value a_{ij} ($a_{ji} = \frac{1}{a_{ij}}$) with judgement scale ranges from 1 to 9 to generate a preference matrix $A = [a_{ij}]$ for decision-making, with 9 representing absolutely importance. Suppose that the dimension of the preference matrix is $n \times n$, w_i can be obtained as the weight for each element after normalization as follows.

$$w_i = \frac{\sum_{j=1}^{n} \frac{a_{ij}}{\sum_{i=1}^{n} a_{ij}}}{\sum_{i=1}^{n} \sum_{j=1}^{n} \frac{a_{ij}}{\sum_{i=1}^{n} a_{ij}}} \tag{8}$$

To check the consistency of the preference matrix, a random consistency index table is utilized to verify the consistency ratio CR by (9) [21]. The consistency can be verified if the value of CR is smaller than 0.1. The size of matrix n has a corresponding random average r. In this paper, $n = 3$, therefore, $r = 0.58$ [22].

$$CR = \frac{\frac{1}{n}\sum_{i=1}^{n}\frac{(Aw)_i}{w_i} - n}{r(n-1)} \tag{9}$$

Table II shows the preference matrix for the Criteria Layer

TABLE II: The Preference Matrix and the Weights

Criteria Layer ($CR = 0.008$)					**Index Layer of C2** ($CR = 0.048$)				
	$\boldsymbol{C_1}$	$\boldsymbol{C_2}$	$\boldsymbol{C_3}$	W_p^C		$\boldsymbol{I_{21}}$	$\boldsymbol{I_{22}}$	$\boldsymbol{I_{23}}$	W_{pq}^I
$\boldsymbol{C_1}$	1	2	3	0.54	$\boldsymbol{I_{21}}$	1	2	4	0.57
$\boldsymbol{C_2}$	1/2	1	2	0.31	$\boldsymbol{I_{22}}$	1/2	1	2	0.29
$\boldsymbol{C_3}$	1/3	1/2	1	0.15	$\boldsymbol{I_{23}}$	1/4	1/2	1	0.14

and the Index Layer of C_2 given by the designer, where W_p^C is the weight for the p_{th} index in the criteria layer, W_{pq}^I is the weight for the q_{th} index in the index layer under the p_{th} criteria layer. Considering that C_1 and C_3 have only one index, W_{11}^I and W_{31}^I are equal to 1. The calculation for the other weights is based on (8). For both the Criteria Layer and the Index Layer of C_2, $CR < 0.10$, which indicates that the consistency of the preference matrix can be ensured. I_{pq} indicates the evaluation value for the q_{th} index of the p_{th} criteria. The EWI is defined as follows:

$$EWI = \sum_{p=1}^{n_c}\sum_{q=1}^{n_p} W_p^C W_{pq}^I \cdot I_{pq} \tag{10}$$

where n_c is the number of metrics in the criteria layer, n_p is the number of metrics in the index layer under the p_{th} metric of the criteria layer. The second and the third column of Table III show the calculation results for the two robots used in the case study, which are obtained through the numerical calculation.

EWI can be used during the configuration selection process when the master manipulator candidates satisfy the equivalent model. Based on these results, it is evident that the spherical robot outperforms the articulated robot, and will be chosen as the basic configuration of master manipulator prototype design for the Hamlyn CRM.

To eliminate the differences brought by the unequal workspace volume when the two robots for comparison do not satisfy the equivalent model during the final prototype verification process, the effective workspace V_e is calculated based on the product of the volume of reachable workspace V and the EWI for design quality evaluation. The weights can be changed based on the designers preference for a specific design target, which means that the proposed framework in this paper can be readily adapted to other robot designs under different requirements.

III. System Design

Based on the proposed framework, this section provides detailed information on the design of the master manipulator, including the structure design and the control system design for the Hamlyn CRM.

TABLE III: Results for Effective Workspace Analysis

		Articulated Robot	**Spherical Robot**	**Phantom Omni**	**Hamlyn CRM**
$\boldsymbol{C_1}$	$\boldsymbol{I_{11}}$	0.807	1.153	0.817	1.042
	$\boldsymbol{I_{21}}$	0.518	0.524	0.553	0.587
$\boldsymbol{C_2}$	$\boldsymbol{I_{22}}$	0.456	0.685	0.524	0.729
	$\boldsymbol{I_{23}}$	0.459	0.680	0.525	0.724
$\boldsymbol{C_3}$	$\boldsymbol{I_{31}}$	0.522	0.538	0.234	0.456
$\boldsymbol{V}(m^3)$		0.034	0.041	0.012	0.037
$\boldsymbol{EWI}$		0.667	0.887	0.644	0.832
$\boldsymbol{V_e}(m^3)$		0.023	0.036	0.008	0.031

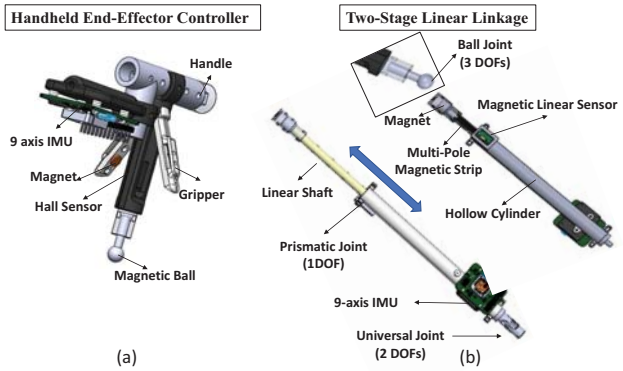

Fig. 5: Details of structure. (a) Handheld end-effector controller, (b) Two-stage linear linkage.

A. Mechanical Structure Design

In this study, a position and orientation decoupling design is employed, so that the translation and orientation components can be independently controlled. The prototype is composed of a handheld end-effector controller to sense the hand's orientation and a two-stage linear linkage with a universal joint and a prismatic joint to sense the hand's position.

As for orientation control, most of the wrist mechanism of the existing manipulators consist of three joints with axes intersected at one point to provide a human wrist like operational flexibility. A gimbal mechanism is widely used to form the orientation control, such as the dVRK Master Tool Manipulators (MTM) and the Phantom Omni. In order to achieve a compact design, ball joints were used for serial rotation as a 3-DoFs joint. It was realized by a magnetic ball connection between the end-effector and the linear linkage. A one-DoF gripper was used to provide gripping motion for the operator, which was mounted on the handle of the handheld end-effector controller.

As for the position control, a universal joint was used as a 2-DoFs joint. Linear motion was generated by a linear shaft and a hollow cylinder. The universal joint and the prismatic joint can form the spherical mechanism. The details of the structure design of the Hamlyn CRM are shown in Fig. 5. The DH table and joint limits of the proposed master manipulator (the Hamlyn CRM) are shown in Table IV.

TABLE IV: DH Table and Joint Limits for the Hamlyn CRM.

	1	2	3	4	5	6
α	0	90	-90	0	-90	90
a	0	0	0	0	0	0
d	0	0	d	0	0	0
θ	θ_1	θ_2	0	θ_4	θ_5	θ_6
θ_u	135	135	0.40	180	160	70
θ_d	45	45	0.24	-180	20	-70

Note: The unit for the angle of the revolute joint is degree.
The unit for the link offset and the joint limits for prismatic joint is metre.

The master manipulator is mounted on an aluminium frame where two calibration docking bases for initializing the position and orientation of the end-effector are installed. The overall moving weight of the master manipulator is minimized to 300g, which is lightweight enough and the gravity compensation is not considered in this prototype.

B. Control System Design

The control system includes motion tracking and master-slave mapping for slave robot control. Based on the DH table (see Table IV) and the forward kinematic, the position vector of the master manipulator end-effector $\boldsymbol{P_e}$=[X_e,Y_e,Z_e] can be obtained as follows.

$$\begin{cases} X_e = -cos(\theta_1)sin(\theta_2)d \\ Y_e = -cos(\theta_2)d \\ Z_e = -sin(\theta_1)sin(\theta_2)d \end{cases} \tag{11}$$

where θ_1 and θ_2 are the two serial rotation angles for the universal joint obtained by the IMU on the linear shaft. d is the total length of the two-stage linkage at a specific point, the value of which is obtained by the linear magnetic sensor. As for the end-effector orientation, the Euler angles can be calculated based on the IMU sensors. In this way, the motion tracking of the 6D pose of the end-effector can be realized.

For master-slave mapping, in pursuit of intuitive teleoperation, the orientation of the slave robot's end-effectors is expected to be the same as the master manipulators end-effectors, while the real-time increment value for position control is scaled down by a fixed motion-scaling ratio τ.

$\boldsymbol{M}$ and $\boldsymbol{G}$ represent the base and the gripper of the master manipulator respectively, while $\boldsymbol{E}$ and $\boldsymbol{S}$ represent the end-effector and the RCM point of the slave robot respectively. After visual cues alignment, $\boldsymbol{T}_S^E$ is the final result that used to control a slave robot. Here we define $\boldsymbol{R}_M^G$ and $\boldsymbol{P}_M^G$ as the rotation matrix and the translation vector that form the homogenous transform matrix $\boldsymbol{T}_M^G$. $\boldsymbol{T}_S^E$ at time step t can be obtained as follows.

$$\boldsymbol{T}_S^E(t) = \begin{bmatrix} \boldsymbol{R}_M^G(t) & \tau(\boldsymbol{P}_M^G(t) - \boldsymbol{P}_M^G(t-1)) \\ \boldsymbol{0} & 1 \end{bmatrix} \tag{12}$$

C. System Integration

In order to verify the effectiveness of the master manipulator proposed in this paper, user studies were conducted on the dVRK [23]. The patient side manipulators (PSMs) were utilized as slave robot. The physical prototype of the Hamlyn CRMm and the slave robot for the user studies are illustrated in Fig. 6. The slave robot consists of two patient side manipulators (PSM1, PSM2) with dVRK controllers, a stereo endoscopic system. A micro-controller (Arm Mbed OS) is used to acquire the sensor's data and fulfil low-level sensor data processing. A foot pedal (Philips LFH2310) is utilized to provide the "engage" and "clutch" information during the remote control, similar to the control console of dVRK.

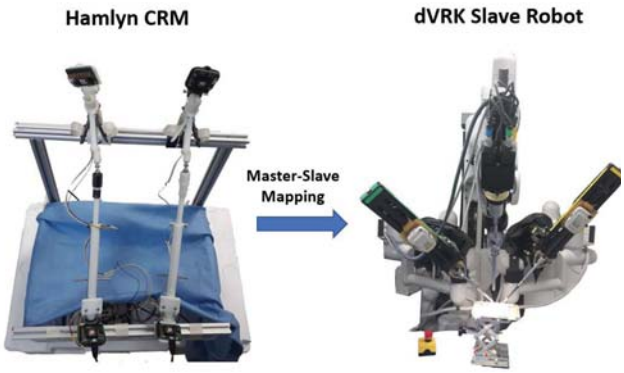

Fig. 6: The physical prototype of the Hamlyn CRM and the dVRK slave robot for user studies.

The software for the whole system is constructed based on a Robotic Operating System (ROS) framework on a Linux Host PC. All the sensor information transmitted by the micro-controller is subscribed as ROS topics, and the high-level sensor fusion and processing are accomplished on the Host PC. The final control commands are generated and published to control the da Vinci robot via the dVRK-ROS Bridge to set the dVRK robot's end-effector Cartesian pose, using the CISST-SAW libraries [23].

IV. Experiments

In this section, the Hamlyn CRM and the Phantom Omni are integrated to the dVRK control console for user studies. Experimental setup and design are illustrated, and the results of the experiments are analyzed.

A. User Studies

The DH parameters and joint limits of the Phantom Omni were introduced in [24], [25]. The design evaluation metrics are provided in the 4_{th} and 5_{th} columns in Table III based on numerical calculation. It can be concluded that the Hamlyn CRM has significantly larger effective workspace V_e compared to the Phantom Omni, which indicates that it has evident advantages for the design quality.

Eight subjects were invited to participate in all the user studies through full procedures (2 females and 6 males; aged 30.13±3.68). One of the participants is an experienced orthopedic surgeon, the others are engineers who specialize in surgical robotics. All the participants are right-handed. Five of the participants had at least one previous experience

in robotic teleoperation, while two of them are familiar with the dVRK controller. Before the user studies, each subject had a practice session to get familiar with the master manipulator before they felt confident to complete the whole task. Subjects were required to use the grippers of the surgical tools to grasp, locate, transfer and place the ring following the pre-defined procedures.

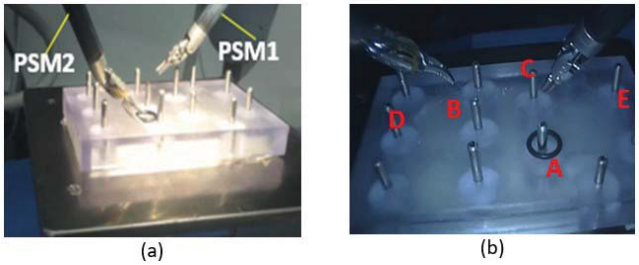

Fig. 7: Illustration of the Ring Transfer Task. (a) Experimental setup, (b) Task description.

Illustration of the ring transfer task is shown in Fig. 7, including the experiment setup and task description. PSM1 and PSM2 represents the right arm and the left arm of the slave robot respectively (see Fig. 7 (a)). The notations of A,B,C,D,E are shown in Fig. 7 (b). The initial position of the right tool is located at A, while the left tool is located at B. Prior to task executions, the tools were controlled by the subject to dock at a suitable pose, which ensures a fair comparison among all the user studies. Once the subjects felt natural with the initial pose, task execution began. The whole procedures for ring transfer task are as follows:

1). Control PSM1 to grasp the ring from A, then transfer and place it on B.

2). Control PSM2 to grasp the ring from B, then transfer and place it on C.

3). Control PSM1 to grasp the ring from C, pass the ring to PSM2, then place the ring on D.

4). Control PSM2 to grasp the ring from D, pass the ring to PSM1, then place the ring on E.

The stereo display screen of the da Vinci control console was used for all the experiments to make sure that the results of user studies are only influenced by the design of the master manipulators. Each subject contributed three to five trials during the user studies. In order to remove outliers, the best trial and worst trial in term of task completion time for each subject were abandoned. A total of 28 trials were collected for statistical analysis.

B. Results and Analysis

For quantitative analysis, four evaluation metrics are used to evaluate the performance of the subjects during teleoperation, including the total path length of the instruments P_i, the task completion time T_c, the average speed of operation A_s, and the number of clutching N_c.

- **Total Path Length of the Instruments** (P_i): The total path length of the surgical instruments generated by the slave robot when conducting a trial.

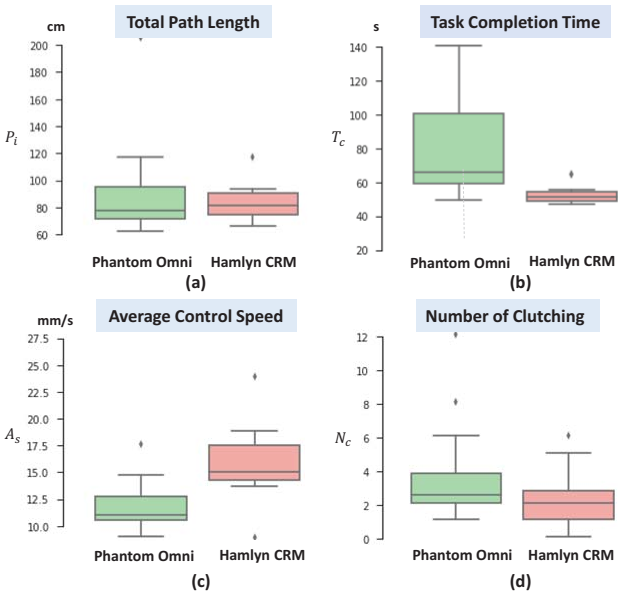

Fig. 8: Results for comparison in the form of box plot. Comparisons in term of (a) $P_i(cm)$; (b) $T_c(s)$; (c)$A_s(mm/s)$; (d) N_c.

- **Task Completion Time** (T_c): The length of the time for a subject to finish the whole procedures of the ring transfer task during one trial.
- **Average Control Speed** (A_s): The ratio between the total path length of the instruments and the task completion time.
- **Number of Clutching** (N_c): The number of the user using clutching mechanism to reposition the end-effector of the master manipulator during an operation.

As the subjects involved have different levels of expertise, unsurprisingly these are reflected in the performance variation. Table V shows the average results and corresponding standard deviation among all the trials for the four evaluation metrics.

TABLE V: User Studies Results

	Phantom Omni	**Hamlyn CRM**	**p-value**
$P_i(cm)$	92.8 $\pm$ 37.1	84.0 $\pm$ 13.1	0.5089
$T_c(s)$	79.0 $\pm$ 28.5	52.7 $\pm$ 5.7	0.0015
$A_s(mm/s)$	11.9 $\pm$ 2.3	15.9 $\pm$ 3.4	0.0013
N_c	3.6 $\pm$ 3.1	2.2 $\pm$ 1.6	0.0202

Among all the performance metrics, it has been shown that the Hamlyn CRM has a relatively short total trajectory of the instruments during operation, and less clutching number and task completion time, compared to the Phantom Omni, while the average speed is higher. This indicates that the performance of the Hamlyn CRM is better than the Phantom Omni among all evaluation metrics. The results for each master manipulator are plotted in a box plot form, as shown in Fig. 8.

Normality tests (Shapiro-Wilk test) at 0.05 significance

level were performed to check if the metrics satisfy the normal distribution assumption. The results indicated that except for A_s, all the metrics reveal non-parametric nature. Wilcoxon signed-rank tests are therefore conducted for non-parametric statistical comparison between variables P_i, T_c and N_c. T test was used for p-value calculation for A_s. The results can be seen in Table V. It can be concluded that P_i does not have significant contribution (p-value = 0.5089 > 0.05) to differentiate the performance of different master manipulators. There are significant differences between the Hamlyn CRM and the Phantom Omni in terms of T_c (p-value = 0.0015 < 0.05), A_s (p-value = 0.0013 < 0.05) and N_c (p-value = 0.0202 < 0.05).

It can be seen that the Hamlyn CRM outperforms Phantom Omni according to the evaluation results for the user studies. The average clutching number and completion time of Phantom Omni are much higher than that of the Hamlyn CMR. Though Phantom Omni is a mature commercial product, the button design reduced the intuitiveness of gripping motion and may have potential influence on the performance, but the results are still valuable to evaluate the overall performance.

V. Conclusions

An effective workspace analysis framework is proposed in this paper to provide decision-support for the design and evaluation of a portable master manipulator with the advantages of compactness, high workspace quality and mapping efficiency. A systematic overview of the Hamlyn CRM is provided by detailing the structure design, motion tracking technique and master-slave mapping.

The prototype is lightweight with reduced complexity and is compact enough to be easily adapted to small control consoles. The design evaluation indicates that the Hamlyn CRM has evident strengths compared to the Phantom Omni.

Detailed user studies on the dVRK illustrate the relative merit of the Hamlyn CRM as compared to the Phantom Omni in terms of the task completion time, average control speed and number of clutching, thus demonstrating the potential clinical value of the device.

Acknowledgement

The authors would like to acknowledge Shen Treratanakulchai and Yang Hu for discussion and helping with 3D printing, would like to thanks to all the subjects involved in the user studies.

References

[1] V. Vitiello, S.-L. Lee, T. P. Cundy, and G.-Z. Yang, "Emerging robotic platforms for minimally invasive surgery," *IEEE reviews in biomedical engineering*, vol. 6, pp. 111–126, 2013.

[2] G.-Z. Yang, J. Bellingham, P. E. Dupont, P. Fischer, L. Floridi, R. Full, N. Jacobstein, V. Kumar, M. McNutt, R. Merrifield, *et al.*, "The grand challenges of science robotics," *Science Robotics*, vol. 3, no. 14, p. eaar7650, 2018.

[3] C. J. Payne and G.-Z. Yang, "Hand-held medical robots," *Annals of biomedical engineering*, vol. 42, no. 8, pp. 1594–1605, 2014.

[4] C. Freschi, V. Ferrari, F. Melfi, M. Ferrari, F. Mosca, and A. Cuschieri, "Technical review of the da vinci surgical telemanipulator," *The International Journal of Medical Robotics and Computer Assisted Surgery*, vol. 9, no. 4, pp. 396–406, 2013.

[5] C. Bergeles and G.-Z. Yang, "From passive tool holders to microsurgeons: safer, smaller, smarter surgical robots," *IEEE Transactions on Biomedical Engineering*, vol. 61, no. 5, pp. 1565–1576, 2014.

[6] P. Berkelman, E. Boidard, P. Cinquin, and J. Troccaz, "Ler: The light endoscope robot," in *Intelligent Robots and Systems, 2003.(IROS 2003). Proceedings. 2003 IEEE/RSJ International Conference on*, vol. 3. IEEE, 2003, pp. 2835–2840.

[7] S.-K. Kim, W.-H. Shin, S.-Y. Ko, J. Kim, and D.-S. Kwon, "Design of a compact 5-dof surgical robot of a spherical mechanism: Cures," in *Advanced Intelligent Mechatronics, 2008. AIM 2008. IEEE/ASME International Conference on*. IEEE, 2008, pp. 990–995.

[8] J. Shang, K. Leibrandt, P. Giataganas, V. Vitiello, C. A. Seneci, P. Wisanuvej, J. Liu, G. Gras, J. Clark, A. Darzi, *et al.*, "A single-port robotic system for transanal microsurgerydesign and validation," *IEEE Robotics and Automation Letters*, vol. 2, no. 3, pp. 1510–1517, 2017.

[9] P. Wisanuvej, G. Gras, K. Leibrandt, P. Giataganas, C. A. Seneci, J. Liu, and G.-Z. Yang, "Master manipulator designed for highly articulated robotic instruments in single access surgery," in *Intelligent Robots and Systems (IROS), 2017 IEEE/RSJ International Conference on*. IEEE, 2017, pp. 209–214.

[10] F. Bovo, G. De Rossi, F. Visentin, *et al.*, "Surgical robot teleoperation with bbz console," *Asvide*, vol. 4, no. 1, 2017.

[11] H. Lee, B. Cheon, M. Hwang, D. Kang, and D.-S. Kwon, "A master manipulator with a remote-center-of-motion kinematic structure for a minimally invasive robotic surgical system," *The International Journal of Medical Robotics and Computer Assisted Surgery*, vol. 14, no. 1, p. e1865, 2018.

[12] S. Kucuk and Z. Bingul, "Comparative study of performance indices for fundamental robot manipulators," *Robotics and Autonomous Systems*, vol. 54, no. 7, pp. 567–573, 2006.

[13] T. Yoshikawa, "Manipulability of robotic mechanisms," *The international journal of Robotics Research*, vol. 4, no. 2, pp. 3–9, 1985.

[14] J.-O. Kim and K. Khosla, "Dexterity measures for design and control of manipulators," in *Intelligent Robots and Systems' 91.'Intelligence for Mechanical Systems, Proceedings IROS'91. IEEE/RSJ International Workshop on*. IEEE, 1991, pp. 758–763.

[15] T. Yoshikawa, *Foundations of robotics: analysis and control*. Mit Press, 1990.

[16] M. J. Tsai and Y. H. Chiou, "Manipulability of manipulators," *Mechanism and Machine Theory*, vol. 25, no. 5, pp. 575–585, 1990.

[17] C. Direkwattana, J. Suthakorn, and C. Wilasrusmee, "Workspace analysis for a new design laparoscopic robotic manipulator," in *MU-LapaRobot1, 20th National Grad Research Conference*, 2011, pp. 2–3.

[18] J. Rosen, J. D. Brown, L. Chang, M. N. Sinanan, and B. Hannaford, "Generalized approach for modeling minimally invasive surgery as a stochastic process using a discrete markov model," *IEEE Transactions on Biomedical engineering*, vol. 53, no. 3, pp. 399–413, 2006.

[19] J. Rosen, J. D. Brown, L. Chang, M. Barreca, M. Sinanan, and B. Hannaford, "The bluedragon-a system for measuring the kinematics and dynamics of minimally invasive surgical tools in-vivo," in *Robotics and Automation, 2002. Proceedings. ICRA'02. IEEE International Conference on*, vol. 2. IEEE, 2002, pp. 1876–1881.

[20] F. Zahedi, "The analytic hierarchy processa survey of the method and its applications," *interfaces*, vol. 16, no. 4, pp. 96–108, 1986.

[21] J. A. Alonso and M. T. Lamata, "Consistency in the analytic hierarchy process: a new approach," *International journal of uncertainty, fuzziness and knowledge-based systems*, vol. 14, no. 04, pp. 445–459, 2006.

[22] A.-L. CHICEA, R.-E. BREAZ, O. Bologa, and S.-G. RACZ, "Using serial industrial robots and cam techniques for manufacturing prosthetic devices." *Applied Mechanics & Materials*, vol. 762, 2015.

[23] P. Kazanzides, Z. Chen, A. Deguet, G. S. Fischer, R. H. Taylor, and S. P. DiMaio, "An open-source research kit for the da vinci® surgical system," in *Robotics and Automation (ICRA), 2014 IEEE International Conference on*. IEEE, 2014, pp. 6434–6439.

[24] A. J. Silva, O. A. D. Ramirez, V. P. Vega, and J. P. O. Oliver, "Phantom omni haptic device: Kinematic and manipulability," in *Electronics, Robotics and Automotive Mechanics Conference, 2009. CERMA'09.* IEEE, 2009, pp. 193–198.

[25] J. San Martin and G. Trivino, "A study of the manipulability of the phantom omni haptic interface." in *VRIPHYS*, 2006, pp. 127–128.